Comparison of Different Quantitative Approaches to ^{18}F-Fluoride PET Scans

Winfried Brenner, MD, PhD[1]; Cheryl Vernon, BS[1]; Mark Muzi, MS[2]; David A. Mankoff, MD, PhD[1]; Jeanne M. Link, PhD[1]; Ernest U. Conrad, MD[3]; and Janet F. Eary, MD[1]

[1]Division of Nuclear Medicine, University of Washington Medical Center, Seattle, Washington; [2]Department of Radiology, University of Washington Medical Center, Seattle, Washington; and [3]Department of Orthopedics, University of Washington Medical Center, Seattle, Washington

The aim of this study was to evaluate the relationship between ^{18}F-fluoride bone metabolic measures obtained by nonlinear regression (NLR), Patlak analysis, and standardized uptake value (SUV) for a wide range of normal and pathologic bone conditions. In patients imaged twice, changes in metabolic rates were determined using the different quantitation methods. **Methods:** In 33 patients 2–51 mo after resection of a bone tumor of the limbs, a total of 42 dynamic PET scans were performed after injection of 250–350 MBq ^{18}F-fluoride. SUV, fluoride bone influx rate obtained by Patlak analysis (K_{Pat}), and fluoride bone influx rate obtained by NLR (K_{NLR}) were calculated in each patient for the bone graft, the contralateral normal side, and the spine, if within the field of view. **Results:** SUV ranged from 0.4 to 9.9, K_{Pat} from 0.0035 to 0.0742 mL/min/mL, and K_{NLR} from 0.0027 to 0.0737 mL/min/mL. Significant linear correlations were found between K_{Pat} and K_{NLR} ($r = 0.99$), K_{Pat} and SUV ($r = 0.95$), and K_{NLR} and SUV ($r = 0.93$). Eight patients have been imaged twice within 6 mo. Changes in metabolic values of the grafts were significantly correlated for K_{Pat} and K_{NLR} ($r = 0.96$), K_{Pat} and SUV ($r = 0.88$), and K_{NLR} and SUV ($r = 0.79$). The 95% ranges of normal change in limb bones were ±58.0% for SUV, ±23.0% for K_{Pat}, and ±20.2% for K_{NLR}; the corresponding 95% ranges in the spine were ±8.6%, ±7.6%, and ±19.6%. **Conclusion:** The results of this study show that ^{18}F-fluoride metabolic values as well as changes in bone metabolism measured by SUV and Patlak analysis were strongly correlated with NLR findings. The high 95% range of normal change of SUV in limb bones, however, indicates that this parameter is of limited value in areas with low metabolic activity. The range of spontaneous bone metabolic rate fluctuations presented in this study may be used as an estimate for assessing changes in bone metabolic activity, and the normal values for limb bones provide a basis for further studies on ^{18}F-fluoride bone metabolism.

Key Words: ^{18}F-fluoride ion; PET; bone metabolism; nonlinear regression; Patlak graphical analysis; standardized uptake value

J Nucl Med 2004; 45:1493–1500

The positron emitter ^{18}F-fluoride has a long history as a tracer for bone imaging. After its introduction by Blau et al. in 1962 (*1*), ^{18}F-fluoride ion became the standard agent for bone scanning until the development of ^{99m}Tc-labeled bisphosphonates in the 1970s. A PET-based kinetic model for ^{18}F-fluoride in human subjects was introduced by Hawkins et al. in 1992 (*2*) and an initial report on the use of ^{18}F-fluoride for whole-body skeletal PET imaging in patients was published by Hoh et al. in 1993 (*3*).

^{18}F-Fluoride is extracted from plasma in proportion to bone perfusion (*4–7*) following a well-described physiologic process that allows quantitative studies of the skeleton with dynamic PET imaging (*7*). Hawkins et al. (*2*) introduced a 3-compartment, 4-parameter kinetic model for ^{18}F-fluoride behavior consisting of the plasma space, an unbound bone compartment, and a bound bone compartment (Fig. 1). In reflecting the physiologic process, the model describes fluoride kinetics from the plasma into the unbound bone compartment and then ionic exchange of the fluoride with hydroxyl groups in hydroxyapatite to form fluoroapatite (bound fraction). The rate constants for these processes can be calculated by standard nonlinear regression (NLR) methods using dynamic PET in combination with arterial blood sampling as the gold standard. According to this compartment model, the ^{18}F-fluoride bone influx rate is used as a measure of bone metabolism (*2,8–11*). As an alternative to NLR, the bone influx rate can also be estimated by Patlak graphical analysis and the results are correlated with the compartmental modeling results (*2,10–12*), although single rate constants are not calculated. Patlak analysis involves linear regression and can be performed more easily and robustly than NLR methods. However, in the daily routine of a PET center, even simplified methods such as Patlak analysis are not used on a regular basis since they require blood sampling and dynamic imaging for determining the input function. The most widely used parameter for quantitation of PET studies in clinical practice is the standardized uptake value (SUV). This semiquantitative measure represents the tissue activity within a region of interest (ROI) corrected for the injected activity and for patient

Received Dec. 11, 2003; revision accepted Jan. 29, 2004.

For correspondence or reprints contact: Winfried Brenner, MD, PhD, Division of Nuclear Medicine, University of Washington Medical Center, 1959 NE Pacific St., Box 356113, Seattle, WA 98195-6113.

E-mail: winbren_2000@yahoo.com

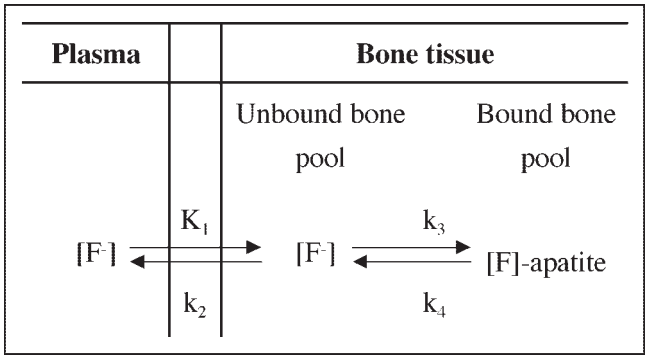

FIGURE 1. Three-compartment, 4-parameter model for fluoride bone metabolism.

weight or lean body mass. The practical advantages of this approach are that static PET images without blood sampling are all that is required. The calculation of SUV requires a transmission scan only to measure true tissue activity in attenuation-corrected images. However, despite the practical usefulness of SUV, to our knowledge, there are no reports that used SUV as the most simple semiquantitative measure for bone metabolism in ^{18}F-fluoride PET.

The aim of this study was to evaluate the relationship between ^{18}F-fluoride bone metabolic measures obtained by NLR analysis as the gold standard, Patlak graphical analysis, and SUV for a wide range of normal and pathologic bone conditions and different bone locations. We calculated these parameters for bone grafts, the contralateral normal side, and the spine, if within the field of view, in patients with a history of resected bone tumors and subsequent bone grafting. In patients imaged twice, the changes in bone metabolic rates were examined for the different quantitation methods.

MATERIALS AND METHODS

Patients

For this study, 33 consecutive patients with tumors of the bones presenting for regular follow-up examinations after tumor resection and bone graft surgery were selected for quantitative ^{18}F-fluoride imaging. Patients gave informed consent for the imaging study by signing forms approved by University of Washington Human Subjects and Radiation Safety Committees. The patients ranged in age from 18 to 65 y and had a wide range of benign (n = 18) and malignant (n = 15) bone tumors. Nine patients were imaged twice, resulting in a total of 42 ^{18}F-fluoride PET scans. Imaging was performed at 2–51 mo (mean, 12 mo) after primary or revision graft surgery. Grafts were located in the humerus (n = 15), the femur (n = 16), the tibia (n = 7), the fibula (n = 2), or the bones of the foot (n = 2). In 14 scans the thoracic spine was within the field of view. None of the patients showed evidence of residual tumor tissue or local relapse. All patients had normal renal function, as ensured by serum creatinine concentrations within the normal range of 0.3–1.2 mg/dL.

Radiopharmaceutical

^{18}F-Fluoride for injection was produced, following United States Pharmacopeia (USP) guidelines, by irradiating ^{18}O-water with protons in a metal target. After bombardment, the target water was passed through a small amount of an anion-exchange resin (Dowex 1X8 [OH^-]; Bio-Rad Laboratories) to trap the ^{18}F-fluoride while the isotopically enriched water was eluted and retained for reuse. ^{18}F-Fluoride was eluted off the resin column with 40–200 μL of 0.5 mol/L sodium bicarbonate solution. This eluate was diluted with 10 mL of sterile isotonic saline and filtered through a 0.2-μm sterilizing filter into a sterile, pyrogen-free vial and checked for pH (pH = 6–8) and particulates. Apyrogenicity was assayed using a *Limulus* amebocyte lysis assay (Associates of Cape Cod Inc.) and sterility was ensured by the USP sterility test method. The radiochemical and chemical purity and specific activity of the product were assayed using an AN300 high-performance liquid chromatography column (Varian) with 0.05 mol/L NaOH mobile phase at room temperature with suppressed conductivity and radioactivity detection.

PET

Imaging studies were performed on an Advance Tomograph (General Electric Medical Systems) operating in a 2-dimensional high-sensitivity mode, with 35 imaging planes per axial field of view of 15 cm (plane thickness, 4.25 mm) and an in-plane resolution of 4–5 mm (4.0-mm axial full width at half maximum at the center of the tomograph) (*13,14*). An intravenous line was placed in each arm: one side for the tracer injection, the other side for venous blood sampling. After the patient was positioned in the tomograph, a 25-min attenuation scan over the graft site was acquired with a ^{68}Ge source. Subsequently, ^{18}F-fluoride in 10 mL of 0.9% saline solution was infused over 1 min with a syringe pump in a standard activity of 3.7 MBq/kg body weight. Simultaneously with the beginning of tracer infusion, a 60-min dynamic sequence of 24 emission scans was started with acquisition times as follows: four 20-s, four 40-s, four 1-min, four 3-min, and eight 5-min frames. Serial venous blood samples were obtained at 1-min intervals up to 10 min after injection, followed by 5 samples at 2-min intervals and 8 samples at 5-min intervals. Blood samples were centrifuged, and plasma was counted on a Cobra well γ-counter (Packard Instrument Co.).

All images underwent correction for random and scattered coincidence events. Each image in the dynamic dataset was corrected for attenuation and physical decay of ^{18}F-fluoride. Images were reconstructed into 128 × 128 matrices per plane by filtered backprojection using a Hanning filter, resulting in a reconstruction resolution of approximately 12 mm for the dynamic images (*13,14*). Cross-calibration of image data and of blood samples was performed on the day of each study by imaging a 500-mL vial containing a known amount of ^{18}F-fluoride and counting aliquots of this standard solution in triplicate in the well counter.

Data Analysis

PET data were analyzed by an ROI approach. Tissue time–activity curves of the graft, the contralateral normal bone, and a thoracic vertebra, if the spine was within the field of view, were generated from the ROI for each image in the dynamic dataset. These data were processed using 3 different techniques: NLR and Patlak graphical analysis, both based on a 3-compartment model, and SUV calculation.

ROIs. The 30- to 60-min summed images were used to guide ROI placement. Circular or elliptic ROIs, ranging in size from 9 to 30 pixels equaling 1.3–4.4 cm^2, were placed over the contact zone between the graft and the original bone, including the area with maximum counts (Fig. 2). Each ROI was applied to 3–6 contig-

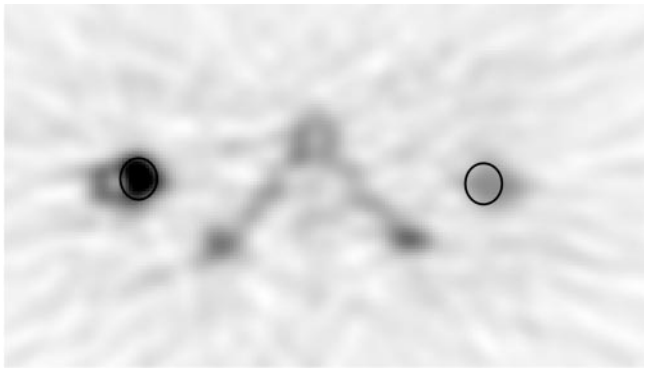

FIGURE 2. Diagram of ROI placement over femoral graft and contralateral normal femur.

uous planes in each frame, creating a volume of interest (VOI). These VOIs limited to a maximum of 6 planes were chosen because we pose that the contact zone with the area of maximum counts reflects graft healing better than a VOI covering the whole graft, which is often a heterogeneous and large area that cannot be completely included within a single tomographic field of view. A same-size VOI was used on the contralateral side as a reference volume for normal bone tissue. For the thoracic vertebrae, VOIs consisting of 3 contiguous planes were created with the ROIs covering the center of the vertebra in each plane. Tissue time–activity curves for all regions were generated from application of the VOIs to the whole dynamic image set. The same VOIs were used for calculating SUV.

SUV. SUV was calculated according to the formula:

$$SUV = \frac{A}{ID/m}, \qquad \text{Eq. 1}$$

where A is the mean tissue activity (μCi/mL or μCi/g) within the VOI in summed images from 30 to 60 min of the dynamic dataset, ID is the injected dose (mCi), and m is the patient body weight (kg).

Patlak Analysis. The fluoride bone influx rate was calculated using graphical analysis (*15,16*) for a 3-compartment model as described by Hawkins et al. (*2*). In Patlak analysis, the fluoride bone influx rate K_{Pat} is determined by the following equation:

$$C_t(t)/C_b(t) = K_{Pat}\left[\int_0^t C_b(t)dt\right]\Big/C_b(t) + V, \qquad \text{Eq. 2}$$

where $C_t(t)$ is the tissue activity concentration (μCi/mL) at time t measured using the ROI approach, $C_b(t)$ is the blood concentration of tracer (μCi/mL), and V is the effective distribution volume of the tracer (mL/mL). K_{Pat} (mL/min/mL; since bone density is different from 1 mg/mL and varies within bones, values are given per milliliter of bone volume instead of per milligram of bone) is the net uptake of fluoride in bone tissue assuming that fluoride in the bound compartment is irreversibly bound to the bones ($k_4 = 0$). K_{Pat} is obtained from the slope of the linear part of the fit of $C_t(t)/C_b(t)$ versus $[\int_0^t C_b(t)dt]/C_b(t)$.

The period before equilibrium of the blood and the exchangeable compartment is characterized as an initial period of curvature before the linear part of the fit. Using the complete dynamic dataset, the linear portion of the curve was observed in almost all patients from 10 to 50 min after injection. These times or, if necessary, individually adjusted times were used as the boundaries for the graphical fit to estimate K_{Pat}. In performing the fit, the time for each point in the tissue time–activity curve was taken as the center of the time bin. Matched time points in $C_b(t)$ were obtained using linear interpolation between neighboring time points in the measured blood curve.

NLR Analysis. NLR was performed on the basis of a 3-compartment model consisting of the plasma space, an unbound bone compartment, and a bound bone compartment (Fig. 1) as described by Hawkins et al. (*2*). The rate constants K_1 to k_4 describe the transport of fluoride between the compartments: K_1 and k_2 for the forward and reverse transport from plasma to the interstitial unbound bone compartment, k_3 for binding to bone apatite, and k_4 for release from the mineral bone compartment. A fifth parameter for the fractional blood volume (fBV) was included to account for the contribution of tracer remaining in the vascular space to the measured tissue data. The delay between tracer injection and tracer accumulation in the bone tissue was estimated by χ^2 fitting in each patient and for each region separately. The blood input function and the time–activity curve data were fitted to this compartment model using a NLR algorithm (PMOD 2.00; PMOD Group, University Hospital Zurich, Zurich, Switzerland) to estimate the kinetic parameters K_1 to k_4 and fBV. For both fBV and K_1–k_3, a parameter range from 0 to 1 was applied, whereas k_4 was constrained to 0–0.1 min^{-1}. Parameter starting conditions for the fit were 0.1 mL/mL, 0.1 mL/min/mL, 0.15 min^{-1}, 0.1 min^{-1}, and 0.01 min^{-1} for fBV, K_1, k_2, k_3, and k_4, respectively. The fluoride bone influx rate K_{NLR} (mL/min/mL) is the net forward transport parameter and was calculated as:

$$K_{NLR} = K_1 \times k_3/(k_2 + k_3). \qquad \text{Eq. 3}$$

Statistical Analysis

Results are given as mean ± 1 SD. For each patient graft, normal bone, and spine, values for SUV and K_{Pat} were plotted against K_{NLR}, and the correlation coefficient was calculated using a spreadsheet program (Excel; Microsoft). The strength of the correlation was judged by the correlation coefficient. The Student t test or ANOVA, each for unpaired datasets, was used to evaluate statistical differences between subgroups, with $P < 0.05$ considered to be statistically significant. In patients imaged twice within 6 mo, the change of the graft metabolic rate as well as the difference between 2 measurements in normal bones and the spine were expressed as a percentage of the initial value. The within-subjects coefficient of variation for repeated PET scans is given for the different quantitation parameters as the percentage of the SD divided by the mean. The 95% range of normal change in patients imaged twice, indicating spontaneous bone metabolic rate fluctuations in normal limb bones and the spine, was calculated as 2 times the SD for each metabolic parameter.

RESULTS

Metabolic measures for ^{18}F-fluoride were obtained in a total of 98 bone sites (42 grafts, 42 normal bone sites of the contralateral limb, and 14 thoracic vertebrae). Results covered a wide range of normal and pathologic values from 0.4 to 9.9, 0.0035 to 0.0742 mL/min/mL, and 0.0027 to 0.0737 mL/min/mL for SUV, Patlak analysis, and NLR, respectively (Table 1). For the relationship between Patlak and NLR, a high linear correlation coefficient of $r = 0.99$ was

TABLE 1
SUV, Patlak (mL/min/mL), and NLR (mL/min/mL) Values for All Bone Locations

Location	*n*	SUV	Patlak	NLR
Grafts	42	5.3 ± 2.2 (1.6–9.9)	0.0346 ± 0.0157 (0.0096–0.0742)	0.0370 ± 0.0165 (0.0106–0.0737)
Normal bones	42	1.4 ± 0.8* (0.4–4.4)	0.0083 ± 0.0048* (0.0035–0.0256)	0.0085 ± 0.0051* (0.0027–0.0278)
Thoracic spine	14	5.9 ± 1.0 (4.3–7.2)	0.0387 ± 0.0069 (0.0264–0.0485)	0.0429 ± 0.0085 (0.0277–0.0541)
All locations	98	3.7 ± 2.5 (0.4–9.9)	0.0239 ± 0.0175 (0.0035–0.0742)	0.0256 ± 0.0190 (0.0027–0.0737)

*Significantly lower than spine values ($P < 0.001$).
Results are given as mean ± 1 SD, and minimum–maximum values are in parentheses.

calculated for the whole range of values, irrespective of the bone site (Fig. 3). Significant positive linear correlations were also found for SUV and Patlak and SUV and NLR (Figs. 4 and 5).

In bone grafts, SUV was 5.3 ± 2.2, K_{Pat} was 0.0346 ± 0.0157 mL/min/mL, and K_{NLR} results were almost identical with 0.0370 ± 0.0165 mL/min/mL (Table 1). Nine patients have been imaged twice at approximately 6 and 12 mo after surgery. During this time period, a decrease of the metabolic bone activity was observed for all 3 parameters in 5 patients with cancellous chip grafts, whereas in 4 patients with full bone grafts the values of these parameters increased (Table 2). The changes of SUV and Patlak, and of SUV and NLR were correlated in a statistically significant positive linear manner (Table 2). The changes measured by Patlak and NLR were also highly correlated ($r = 0.96$).

In 14 scans of patients with humerus grafts, the thoracic spine was within the dynamic field of view, allowing calculation of metabolic activity in a vertebra. The mean values for SUV, Patlak, and NLR were 5.9 ± 1.0, 0.0387 ± 0.0069 mL/min/mL, and 0.0429 ± 0.0085 mL/min/mL, respectively (Table 1). In 3 patients imaged twice within 6 mo, metabolic measures for the thoracic spine, irrespective of the calculation method, showed no major changes over time. The relative differences between 2 measurements were 4.3% ± 4.3% for SUV, 6.5% ± 3.8% for Patlak, and 9.0% ± 9.8% for NLR, resulting in within-subjects coefficients of variation of 8.8%, 13.5%, and 13.9%, respectively. The 95% ranges of normal change were ±8.6%, ±7.6%, and ±19.6% for SUV, Patlak, and NLR, respectively.

The contralateral site of the graft was chosen in each patient as the reference normal value for the respective bone. Results for all 3 parameters are summarized in Table 3. Most of the imaged areas were either in the femur, the humerus, or the tibia. ANOVA showed significant differences between these 3 locations for SUV, Patlak, and NLR.

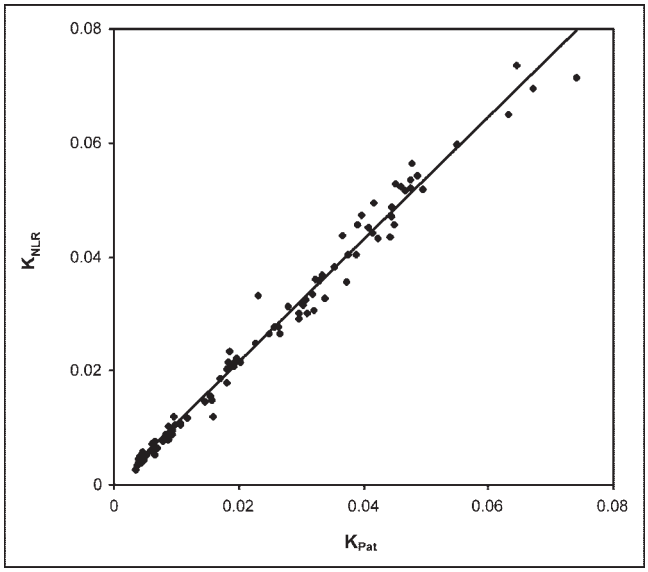

FIGURE 3. Positive linear correlation of K_{Pat} (mL/min/mL) and K_{NLR} (mL/min/mL) for ^{18}F-fluoride ($K_{NLR} = 1.0731\ K_{Pat}$; $r = 0.99$; $P < 0.01$).

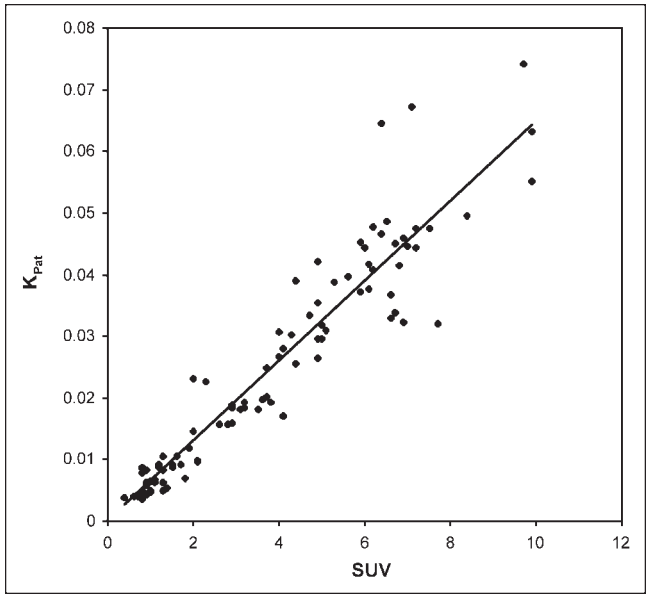

FIGURE 4. Positive linear correlation of SUV and K_{Pat} (mL/min/mL) for ^{18}F-fluoride ($K_{Pat} = 0.0065$ SUV; $r = 0.95$; $P < 0.01$).

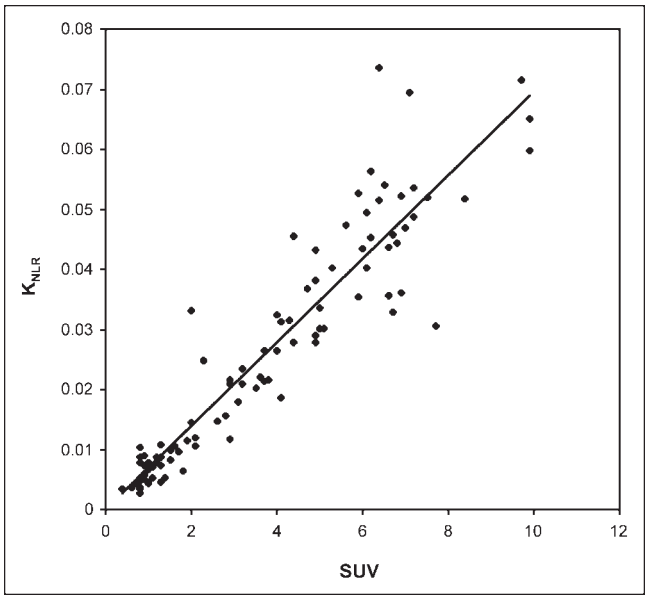

FIGURE 5. Positive linear correlation of SUV and K_{NLR} (mL/min/mL) for ^{18}F-fluoride ($K_{NLR} = 0.0070$ SUV; $r = 0.93$; $P < 0.01$).

The mean metabolic values for the humerus were significantly lower than those in the femur or the tibia for all 3 quantitation methods, whereas no significant differences were found between the femur and the tibia (Table 3). Metabolic values of all limb bones, irrespective of their location, were significantly lower than the values of the thoracic spine (Table 1). For 9 patients imaged twice, the relative changes in normal bones between 2 measurements are summarized in Table 4. The within-subjects coefficients of variation were 75.0% for SUV, 79.0% for K_{Pat}, and 82.5% for K_{NLR}; the corresponding 95% ranges of normal change were ±57.2%, ±27.6%, and ±28.8%. After exclusion of 1 patient who was imaged the second time 30 mo after the first PET scan, the respective 95% ranges of normal change within 6 mo were ±58.0%, ±23.0%, and ±20.2%. ANOVA showed no significant differences between the 3 calculation methods. Differences between 2 measurements were evenly scattered, both in the negative and in the

TABLE 2
Changes in Graft Fluoride Metabolic Values Between 6 and 12 Months After Surgery

SUV	Patlak	NLR
−48.8	−44.0	−35.6
−52.2	−45.4	−28.8
−8.3	−35.4	−40.9
−27.3	−19.3	−18.2
−10.7	−5.6	−12.1
2.5	4.9	17.5
22.0	27.0	33.9
10.3	21.2	19.2
24.1	3.9	5.8

Results are % of baseline values at 6 mo after surgery.

Significant correlations were found between SUV and Patlak ($r = 0.88$; $P < 0.01$), SUV and NLR ($r = 0.79$; $P < 0.02$), and Patlak and NLR ($r = 0.96$; $P < 0.01$).

TABLE 3
SUV, Patlak (mL/min/mL), and NLR (mL/min/mL) Normal Values for Different Limb Locations

Location	SUV	Patlak	NLR
Calcaneous	1.5	0.0086	0.0082
Metatarsal	1.9	0.0118	0.0116
Fibula	0.8	0.0038	0.0034
Fibula	0.8	0.0044	0.0037
Femur	1.4	0.0053	0.0053
Femur	0.9	0.0042	0.0050
Femur	1.3	0.0062	0.0073
Femur	0.9	0.0063	0.0074
Femur	3.1	0.0181	0.0179
Femur	0.9	0.0062	0.0061
Femur	0.7	0.0039	0.0044
Femur	1.3	0.0083	0.0088
Femur	0.8	0.0078	0.0077
Femur	2.8	0.0156	0.0155
Femur	2.6	0.0156	0.0148
Femur	1.7	0.0093	0.0096
Femur	3.7	0.0203	0.0215
Femur	4.4	0.0256	0.0278
Femur	0.8	0.0050	0.0053
Femur	0.8	0.0048	0.0049
Mean	1.8	0.0102	0.0106
SD	1.2	0.0067	0.0069
Humerus	1.5	0.0091	0.0098
Humerus	1.2	0.0093	0.0088
Humerus	1	0.0066	0.0077
Humerus	0.9	0.0058	0.0059
Humerus	1.1	0.0066	0.0052
Humerus	1	0.0049	0.0044
Humerus	1.3	0.0048	0.0046
Humerus	1	0.0048	0.0046
Humerus	0.8	0.0084	0.0088
Humerus	1	0.0065	0.0067
Humerus	1.2	0.0087	0.0079
Humerus	0.9	0.0046	0.0058
Humerus	0.8	0.0035	0.0027
Humerus	0.6	0.0039	0.0038
Humerus	0.4	0.0038	0.0035
Mean	1.0*	0.0061*	0.0060*
SD	0.3	0.0020	0.0022
Tibia	2.1	0.0098	0.0106
Tibia	0.8	0.0088	0.0103
Tibia	1.3	0.0106	0.0107
Tibia	2	0.0145	0.0146
Tibia	1.1	0.0063	0.0072
Tibia	1.8	0.0070	0.0064
Tibia	0.9	0.0083	0.0089
Mean	1.4	0.0093	0.0098
SD	0.5	0.0027	0.0027

*Significantly lower than femur and tibia values ($P < 0.05$).

TABLE 4
SUV, Patlak (mL/min/mL), and NLR (mL/min/mL) Values and Relative Change (%) Between 2 Scans for Normal Limb Bones Imaged Twice

	Time (mo)	Location	SUV	Change (%)	Patlak	Change (%)	NLR	Change (%)
Scan 1		Femur	3.7		0.0203		0.0215	
Scan 2	30	Femur	4.4	17.3	0.0256	23.4	0.0278	25.6
Scan 1		Femur	1.4		0.0053		0.0053	
Scan 2	6	Femur	0.9	−43.5	0.0042	−22.6	0.0050	−5.1
Scan 1		Femur	2.8		0.0156		0.0155	
Scan 2	5	Femur	2.6	−7.4	0.0156	−0.5	0.0148	−4.9
Scan 1		Femur	0.8		0.0050		0.0053	
Scan 2	7	Femur	0.8	0	0.0048	−5.1	0.0049	−7.6
Scan 1		Humerus	1.3		0.0048		0.0046	
Scan 2	7	Humerus	1	−26.1	0.0047	−1.3	0.0046	0.0
Scan 1		Humerus	0.6		0.0039		0.0038	
Scan 2	5	Humerus	0.4	−40.0	0.0038	−2.6	0.0035	−8.2
Scan 1		Humerus	1		0.0066		0.0077	
Scan 2	6	Humerus	0.9	−10.5	0.0058	−11.9	0.0059	−26.8
Scan 1		Tibia	1.1		0.0063		0.0072	
Scan 2	5	Tibia	1.8	48.3	0.0070	9.8	0.0064	−11.2
Scan 1		Fibula	0.8		0.0038		0.0034	
Scan 2	5	Fibula	0.8	0	0.0044	14.0	0.0037	8.5
Mean				−6.9*		0.3*		−3.3*
SD				28.6		13.8		14.4

*Not significantly different (ANOVA; $P > 0.05$).
Time = time difference between 2 scans.
Significant correlations were found between SUV and Patlak ($r = 0.68$; $P < 0.5$) and Patlak and NLR ($r = 0.70$; $P < 0.5$). SUV and NLR were not significantly correlated ($r = 0.17$; $P > 0.5$).

positive direction, with a positive linear correlation between SUV and Patlak and between Patlak and NLR (Table 4). In only 1 patient, a discrepancy between the different methods was found with a decreasing K_{NLR} on the second scan while both SUV and K_{Pat} increased.

DISCUSSION

In a recent report by Cook et al. on skeletal kinetics measured by ^{18}F-fluoride PET, the authors demanded further studies on computationally simplier methods such as SUV and Patlak graphical analysis to see whether these methods are as robust as NLR analysis (*8*). According to our knowledge, however, there are no publications applying SUV as the most simple semiquantitative measure for bone metabolism in ^{18}F-fluoride PET.

Imaging patients who had undergone resection of bony tumors of the limbs followed by bone grafting allowed us to calculate SUV and fluoride flux constants based on Patlak and NLR analysis that covered a wide range of pathologic as well as normal bone conditions of the contralateral side. K_{NLR} ranged from 0.0027 to 0.0737 mL/min/mL. ^{18}F-fluoride flux values obtained by Patlak analysis were almost identical with a highly significant positive linear correlation (Fig. 3). K_{NLR} values were higher than K_{Pat} values in most patients, as already reported in literature (*2,10,11*). The mean difference between K_{NLR} and K_{Pat} was 7% in our study with a slope of 1.07 for the regression line. Beside other factors based on the fitting model, such as inclusion of fBV or other correction parameters, the reason for the difference is that Patlak graphical analysis does not account for the release of ^{18}F-fluoride from the bones represented by the kinetic rate constant k_4, which was greater than zero in almost all our patients (range, $0-0.0256\ min^{-1}$). Therefore, the net forward constant K_{NLR} is expected to be higher than any net forward parameter obviating k_4 effects such as the Patlak approach. The difference between NLR and Patlak fluxes should increase with k_4 contribution. Accordingly, the mean difference between Patlak and NLR was the highest in the spine and in high-uptake grafts that also showed the highest k_4 values of all bones (data not shown).

Clinically more important is the fact that in 9 patients imaged twice, usually at 6 and 12 mo after surgery, the changes in graft metabolic values showed a strong correlation between NLR and Patlak analysis, with a correlation coefficient of 0.96. Changes of K_{Pat} values paralleled changes of K_{NLR} in all grafts (Table 2), suggesting that K_{Pat} is as clinically useful as K_{NLR} for assessing changes in bone metabolism in terms of fluoride bone influx rates. However, NLR also estimates the rate constants K_1 to k_4, information that cannot be provided by Patlak analysis. K_1, for example, is the product of regional blood flow and the extraction fraction of fluoride ion, which can be used as an indirect

measure to estimate bone blood flow (*10,12,17*). Whether these rate constants contain relevant or even essential clinical information is not yet clear. Further studies on normal and complicated bone graft healing with repeated imaging up to 24 mo after surgery will show the clinical significance of the different methods and parameters.

For SUV, we found a similar strong positive linear correlation with NLR ($r = 0.93$). For any clinical application of SUV as an easy-to-obtain substitute for NLR or Patlak analysis, not only a close correlation of SUV and NLR values is necessary, but even more the correlation of changes in patients imaged repeatedly. In 9 grafts imaged twice, the percentage change of metabolic values was significantly correlated between SUV and NLR. In all patients with an increase of K_{NLR}, SUV increased as well, whereas in all patients with decreasing K_{NLR} this decrease was paralleled by SUV (Table 2). Similar findings were obtained for the changes observed in normal limb bones (Table 4) and in the thoracic spine. In 3 patients, the spine was imaged twice, and changes in K_{NLR} were paralleled by changes in SUV in all cases. The same was found for normal bone values. Only in 1 of 9 patients, NLR indicated a decrease of the metabolic activity while SUV increased. In this patient Patlak analysis also indicated an increasing metabolic bone activity while NLR was the only parameter revealing a decrease. The reason for this discordance was a nonoptimal fit in the NLR approach due to a low-peaking and widened blood input function in the second study. During the fitting process, k_4 hit the parameter limits and went to zero, which resulted in a lower K_{NLR} compared with the first study, indicating a decrease in metabolic activity over time. This shows the pitfalls of NLR with its susceptibility to noise in the data and to parameter constraints, whereas SUV as a static parameter and the more robust linear regression approach of Patlak analysis are not affected, or only little affected, by improper input functions.

For any quantitation method, reproducibility of measurements and normal fluctuations of the respective parameter over time are of special interest. Repeated dynamic PET imaging and measurements of bone metabolic parameters within a few days would be necessary to assess the reliability of measurements. Since this is not easy to achieve for radiation safety reasons, and since changes in bone metabolism are usually monitored within an interval of several months, we calculated relative changes in normal bones within 6 mo to assess the constancy of ^{18}F-fluoride bone metabolism. For this reason we compared the results obtained in 8 contralateral normal limb bones and 3 thoracic vertebrae in 8 patients imaged twice within 5–7 mo. In these patients, no bone metabolic relevant treatment was performed between the 2 scans. In the spine, we found a within-subjects coefficient of variation ranging from 8.8% for SUV to 13.9% for NLR. The 95% range of normal change—that is, the range of spontaneous bone metabolic fluctuations—was ±8.6% for SUV, ±7.6% for K_{Pat}, and ±19.6% for K_{NLR}. This means, that changes of >20% within 6 mo would be outside the 95% range of normal change in the spine and could be considered true changes in bone metabolic activity. However, the magnitude of relative changes depends on the initial value of the parameter. For normal limb bones we observed much lower metabolic values for all 3 parameters. The 95% range of normal change within 6 mo was ±58.0% for SUV, ±23.0% for Patlak, and ±20.2% for NLR. Thus, in limb bones, changes of >25% within 6 mo could be considered true changes in the case of K_{Pat} and K_{NLR}, whereas for SUV changes of at least 50% would be required in limb bones to be judged as true changes in metabolic activity. These findings suggest that metabolic changes indicated by SUV in normal-to high-uptake areas such as the spine have clinical importance similar to the changes observed by K_{NLR}. The limitations of SUV, however, become eminent in low-uptake areas, where a relatively greater fraction of the measured activity within the ROI is due to blood activity and unbound ^{18}F-fluoride and, thus, subject to non–bone-related effects that increase the variability in repeated measurements. Such effects have already been described for ^{18}F-FDG (*18*).

It is important to keep in mind that our data on repeated measurements are not estimates for the mere methodologic reproducibility of the different methods comparing 2 single measurements within a few days—and, thus under almost identical conditions—but also reflect normal fluctuations in bone metabolism within a time period of 5–7 mo. Furthermore, the 95% ranges of normal change provided in this study represent only rough estimates based on repeated measurements in 3 vertebrae and 8 limb bones. In the current ^{18}F-fluoride literature there are no patient data for comparison. Only Piert et al. (*12*) reported on phantom measurements for the hip with ^{18}F-fluoride, in which they found coefficients of variation increasing from 5% to 16% with decreasing activities. These values are in a range similar to our values for the spine, and they confirm the observation of higher coefficients of variation with decreasing ^{18}F-fluoride activity—that is, lower metabolic values. Similar findings were reported by Weber et al. for ^{18}F-FDG PET. In patients without treatment, changes in SUV of >20% were outside the 95% range of spontaneous normal change for a mean SUV of 5 (comparable to our values of spine and grafts), whereas for lower SUV a sharp incline of the 95% range up to ±50% and more for SUV values < 1.5 (comparable to our values of normal bones) was observed (*19*).

Whether the findings for normal changes of bone metabolic activity in limb bones are also applicable in limb grafts is not yet clear. Grafts usually had a much higher initial metabolic activity than limb bones, with the mean graft values of SUV, Patlak, and NLR quite similar to those of the spine. Thus, coefficients of variation in grafts may be comparable to the spine rather than to limb bones. According to the findings in the spine, a 20% change of metabolic bone activity might be indicative of true changes in graft metabolism.

Although venous blood sampling tends to overestimate fluoride bone flux by approximately 5% due to a systematic underestimation of blood activity (*20*), mean Patlak and NLR flux values of the thoracic spine were exactly within the range reported in the literature (*8,10*). For limb bones we found significantly lower values than those for the spine (Table 1). For all 3 metabolic parameters, mean values of the humerus, tibia, and femur were only about 15%–25% of the values of the spine. This primarily reflects bone physiology: Since bone turnover in cortical bones is much lower than that in trabecular bones, fluoride uptake values are expected to be low in limb bones due to their relative small portion of trabecular bone (*21,22*). This will be even more pronounced in the predominantly cortical shaft section of limb bones (*23*), as measured in our patients in whom the ROIs were usually placed at the midbone end of the graft and the respective location on the contralateral normal side. However, to some extent, partial-volume effects also account for the low values in the limb bones since we did not correct for these effects. According to the partial-volume recovery data of our PET scanner, object or ROI sizes of $>$1.3 cm, as used in this study, result in a recovery coefficient of $\geq$60% (unpublished data).

CONCLUSION

^{18}F-Fluoride bone metabolic values and percentage changes over time, obtained by SUV and Patlak graphical analysis, were both strongly correlated with NLR values, suggesting that metabolic changes indicated by these 2 parameters have an importance similar to changes in bone metabolism observed by NLR. However, in low-uptake areas such as limb bones, SUV measurements are less reliable than Patlak or NLR analysis, requiring at least changes of $>$50% to be assessed as true metabolic changes rather than spontaneous fluctuations. Thus, SUV seems to be limited to high-uptake areas such as the spine while it does not seem to be an appropriate tool to monitor metabolic changes in limb bones. Patlak analysis was highly linked to NLR over the whole range of physiologic and pathologic metabolic bone activity. Since it is computationally simplier than NLR, it might be the tool of choice to monitor fluoride bone metabolism irrespective of location. Its use would be greatly encouraged by implementing ready-to-use software to calculate Patlak flux values on standard PET systems. NLR, on the other side, provides the most quantitative information due to the possibility to calculate single rate constants and estimate bone blood flow, though the clinical value of these rate constants is still unclear. The 95% ranges of normal change in fluoride metabolic rates provided in this study may be used as an estimate for assessing changes in bone metabolic activity—for example, in healing bone grafts. Furthermore, the normal values for various bones of the limbs provide a basis for further studies on ^{18}F-fluoride bone metabolism.

ACKNOWLEDGMENTS

The authors thank Dr. Kenneth A. Krohn for fruitful discussions and a thorough review of this paper. This study was supported by National Institutes of Health grant R01-CA65537.

REFERENCES

1. Blau M, Nagler W, Bender MA. A new isotope for bone scanning. *J Nucl Med.* 1962;3:332–334.
2. Hawkins RA, Choi Y, Huang SC, et al. Evaluation of the skeletal kinetics of fluorine-18-fluoride ion with PET. *J Nucl Med.* 1992;33:633–642.
3. Hoh CK, Hawkins RA, Dahlbom M, et al. Whole body skeletal imaging with [^{18}F]fluoride ion and PET. *J Comput Assist Tomogr.* 1993;17:34–41.
4. Green JR, Reeve J, Tellez M, Veall N, Wootton R. Skeletal blood flow in metabolic disorders of the skeleton. *Bone.* 1987;8:293–297.
5. Wootton R, Dore C. The single-passage extraction of ^{18}F in rabbit bone. *Clin Phys Physiol Meas.* 1986;7:333–343.
6. Garnett ES, Bowen BM, Coates G, Nahmias C. An analysis of factors which influence the local accumulation of bone-seeking radiopharmaceuticals. *Invest Radiol.* 1975;10:564–568.
7. Nahmias C, Cockshott WP, Belbeck LW, Garnett ES. Measurement of absolute bone blood flow by positron emission tomography. *Skeletal Radiol.* 1986;15:198–200.
8. Cook GJ, Lodge MA, Blake GM, Marsden PK, Fogelman I. Differences in skeletal kinetics between vertebral and humeral bone measured by ^{18}F-fluoride positron emission tomography in postmenopausal women. *J Bone Miner Res.* 2000;15:763–769.
9. Schiepers C, Nuyts J, Bormans G, et al. Fluoride kinetics of the axial skeleton measured in vivo with fluorine-18-fluoride PET. *J Nucl Med.* 1997;38:1970–1976.
10. Berding G, Burchert W, van den Hoff J, et al. Evaluation of the incorporation of bone grafts used in maxillofacial surgery with [^{18}F]fluoride ion and dynamic positron emission tomography. *Eur J Nucl Med.* 1995;22:1133–1140.
11. Piert M, Zittel TT, Becker GA, et al. Assessment of porcine bone metabolism by dynamic [^{18}F]fluoride ion PET: correlation with bone histomorphometry. *J Nucl Med.* 2001;42:1091–1100.
12. Piert M, Winter E, Becker GA, et al. Allogenic bone graft viability after hip revision arthroplasty assessed by dynamic [^{18}F]fluoride ion positron emission tomography. *Eur J Nucl Med.* 1999;26:615–624.
13. DeGrado TR, Turkington TG, Williams JJ, et al. Performance characteristics of a whole-body PET scanner. *J Nucl Med.* 1994;35:1398–1406.
14. Lewellen TK, Kohlmeyer S, Miyaoka R, Schubert S, Stearns C. Investigation of the count rate performance of the General Electric Advance positron emission tomograph. *IEEE Trans Nucl Sci.* 1995;42:1051–1057.
15. Gjedde A. Calculation of cerebral glucose phosphorylation from brain uptake of glucose analogs in vivo: a reexamination. *Brain Res.* 1982;257:237–274.
16. Patlak CS, Blasberg RG, Fenstermacher JD. Graphical evaluation of blood-to-brain transfer constants from multiple-time uptake data. *J Cereb Blood Flow Metab.* 1983;3:1–7.
17. Piert M, Zittel TT, Machulla HJ, et al. Blood flow measurements with [^{15}O]H_2O and [^{18}F]fluoride ion PET in porcine vertebrae. *J Bone Miner Res.* 1998;13:1328–1336.
18. Mankoff DA, Muzi M, Krohn KA. Quantitative positron emission tomography imaging to measure tumor response to therapy: what is the best method? *Mol Imaging Biol.* 2003;5:281–285.
19. Weber WA, Ziegler SI, Thodtmann R, Hanauske AR, Schwaiger M. Reproducibility of metabolic measurements in malignant tumors using FDG PET. *J Nucl Med.* 1999;40:1771–1777.
20. Brenner W, Kampen WU, Müller H, et al. F-18 fluoride PET in minipigs with defined disorders of bone metabolism [abstract]. *J Nucl Med.* 2002;43(suppl):340P.
21. Gross PM, Marcus ML, Heistad DD. Measurement of blood flow to bone and marrow in experimental animals by means of the microsphere technique. *J Bone Joint Surg Am.* 1981;63:1028–1031.
22. Morris MA, Kelly PJ. Use of tracer microspheres to measure bone blood flow in conscious dogs. *Calcif Tissue Int.* 1980;32:69–76.
23. Whiteside LA, Lesker PA, Simmons DJ. Measurement of regional bone and bone marrow blood flow in the rabbit using the hydrogen washout technique. *Clin Orthop.* 1977;122:340–346.

The Journal of NUCLEAR MEDICINE

Comparison of Different Quantitative Approaches to ^{18}F-Fluoride PET Scans

Winfried Brenner, Cheryl Vernon, Mark Muzi, David A. Mankoff, Jeanne M. Link, Ernest U. Conrad and Janet F. Eary

J Nucl Med. 2004;45:1493-1500.

The Journal of Nuclear Medicine is published monthly.
SNMMI | Society of Nuclear Medicine and Molecular Imaging
1850 Samuel Morse Drive, Reston, VA 20190.
(Print ISSN: 0161-5505, Online ISSN: 2159-662X)

SNMMI SOCIETY OF NUCLEAR MEDICINE AND MOLECULAR IMAGING